

Seasonal variations of the solar radiation scattered from the putative dust rings of Mars: a possible basis for photometric searches

M.I. Błęcka and A. Jurewicz

Space Research Centre, Polish Academy of Sciences, ul. Bartycka 18a, 00-716 Warsaw, Poland (e-mail: mib@cbk.waw.pl, aaj@cbk.waw.pl)

Received 9 October 1997 / Accepted 13 May 1998

Abstract. The continuous bombardment of the Martian moonlets Phobos and Deimos by the interplanetary flux of micrometeoroids is believed to produce ejecta, a part of which could be introduced on long-lived circummartian orbits and form tenuous dust rings around the planet. This view is supported by a number of theoretical studies which yield a detailed space structure of the dust rings. There is, however, no direct evidence as to the existence of such rings. We assess the possibility of photometric search after the rings by modelling the field of solar radiance scattered by the putative dust region. The number density distribution of the dust grains around Mars and their size distribution are drawn from the recent theoretical models. The single-scattering albedo of the individual grains is deduced from the reflectance spectra of Phobos, gathered by the spacecraft Phobos 2. A few phenomenological scattering phase functions are taken into account. The largest calculated radiance scattered in the spectral range $0.35 \mu\text{m} - 1.0 \mu\text{m}$ results to be of the order $10^{-6} \text{ W cm}^{-2} \text{ sr}^{-1}$.

Key words: techniques: photometric – planets and satellites: Deimos, Mars, Phobos

1. Introduction

The existence of the dust belts around Mars seems supported very well theoretically, yet they bear the dubious distinction of being the longest studied planetary rings whose existence still has to be verified (Hamilton 1996). The continuous bombardment of the Martian moonlets Phobos and Deimos by micrometeoroids is believed to produce ejecta, a part of which could be put on long-lived circummartian orbits. This view is supported by theoretical studies of the motion of ejecta, which achieved a high degree of refinement (Krivov & Hamilton 1997). As a result, the distributions of grains of various sizes in the space neighbouring Mars, as well as their seasonal changes, have been predicted in detail. On the contrary, the assessments regarding absolute number densities in the dust region are by far less accurate because little is known about the properties of Phobos' and Deimos' regoliths (Krivov & Hamilton 1997). The optical

properties of the grains remain largely unknown (Murchie & Erard 1996; Ksanfomality & Moroz 1995). On one hand, the available data are insufficient to allow returning the refractive indices of the grains, and on the other, the existing reflectance spectra indicate that there seems to be no known spectral analogues of the Phobos' surface layer. We have therefore to rely on indirect methods in assessing the required optical properties on the basis of the existing information.

The present paper addresses the question of searches after the circummartian dust by photometric methods, i.e. by examining the field of solar radiance scattered by the grains. To this purpose we construct a solution of the equation of radiative transfer through the dust region in question. The shape and optical characteristics of the latter are drawn from the theoretical models and plausible hypotheses as mentioned in the foregoing. We focus on the study of the solar light scattered to the Martian equatorial plane. Searches in this plane seem the most promising since it coincides with the symmetry plane of the thin but otherwise extended dust region filled with particles originating from Phobos. This particular spatial configuration can not be handled within the most exploited approach based on an approximation of the scattering medium by a series of infinite, plane parallel adjacent layers because that approach leads to singular expressions (Dones et al. 1993). For this reason we made use of the code LOWTRAN (Kneizys et al. 1983) originally designed to calculate terrestrial atmospheric radiance along a path including Earth's curvature.

The necessary details of the theoretical space distribution of the circummartian dust grains originating from Phobos and Deimos are given in the next section. What can be plausibly assumed about the scattering properties of the individual dust grains on the ground of the existing data is presented in Sect. 3. The details of exploiting LOWTRAN are explained in Sect. 4. The results and conclusions are discussed in Sects. 5 and 6.

2. Distribution of the dust grains in size and space

Theoretical studies on the putative rings of Mars have accumulated to a rich literature on the subject (Krivov & Hamilton 1997, and references therein).

The theoretically analysed circummartian dust area is expected composed of a few distinct populations depending on

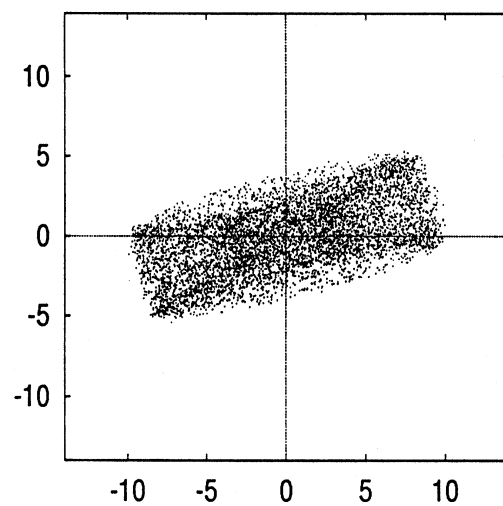
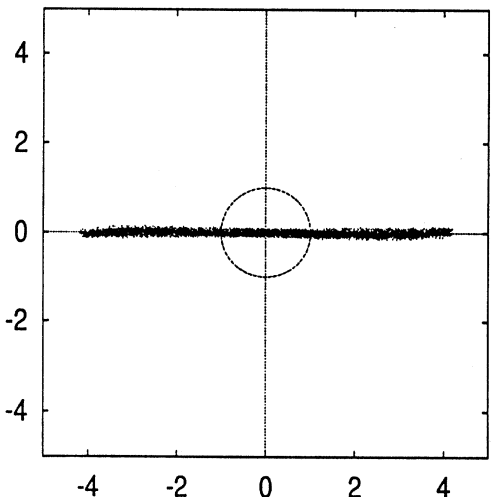
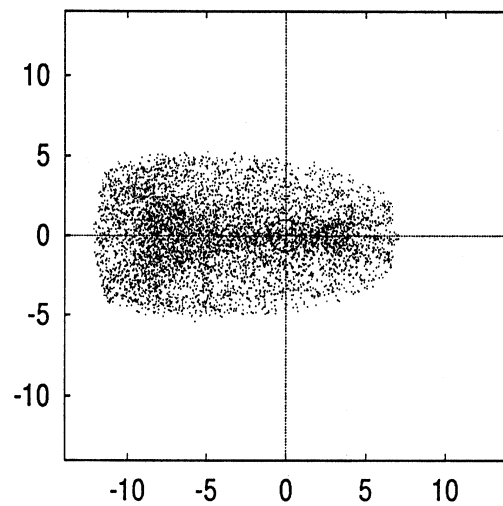
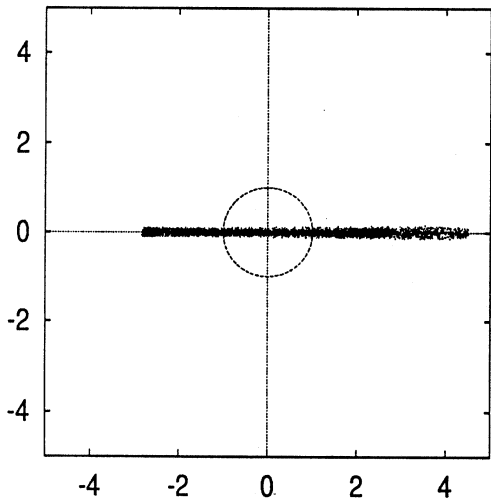
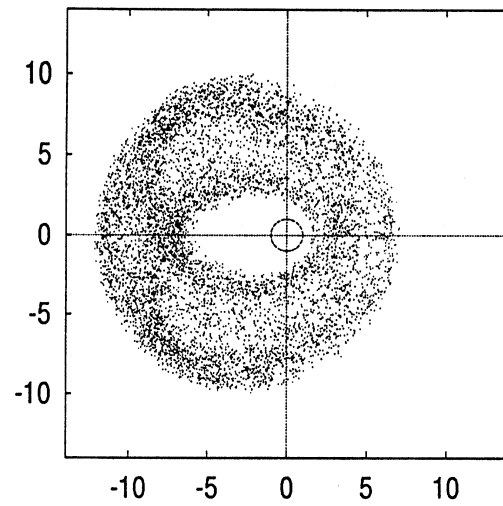
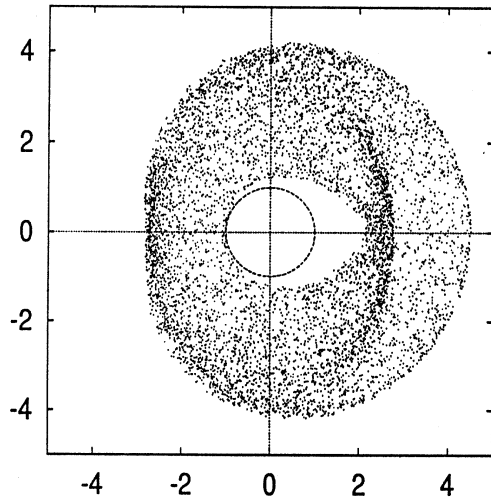


Fig. 1. Projections of the Phobos' torus formed by $32\ \mu\text{m}$ particles at the vernal equinox (XY , XZ and YZ projections from top to bottom). The right-hand coordinate system is inertial and Mars-centered. The X (horizontal) axis points towards the Martian vernal equinox. The Z (vertical) axis points towards the Martian N pole. Distance unit is Martian radius (after Krivov & Hamilton 1997, by courtesy of A. V. Krivov)

Fig. 2. Same as Fig. 1 but for the Deimos' torus formed by $17\ \mu\text{m}$ particles

the forces perturbing the Keplerian motion of a grain (Krivov et al. 1996). The particles with sizes of the order from 10 to $10^2 \mu\text{m}$ form the population most important to the present study, because it is long-lived (the life of an individual grain ranges from tens to tens of thousands of years in orbit) and most numerous (Krivov 1994), hence giving probably the main contribution to the scattering of the solar radiation. The primary perturbing force is here the coupling of solar radiation pressure with the force originating from Mars' oblateness.

In the following, we fix then our attention on the grains with sizes from about 10 to $100 \mu\text{m}$. The shape and internal structure of the dust areas filled with these grains can be described briefly as follows.

The Phobos belt is very flat, and rather ring-shaped than toroidal. Its approximate axis of symmetry is perpendicular to the equatorial plane of Mars, and offset toward the Sun, as shown in Fig. 1. The Deimos belt is extended along its approximate symmetry axis, which is offset away from the Sun and tilted by an angle ranging from 87° for $80 \mu\text{m}$ grains to about 72° for $17 \mu\text{m}$ grains, with respect to the equatorial plane of Mars. An example of the Deimos belt is shown in Fig. 2. The number density distribution of grains in both belts exhibits seasonal dependence when observed in the inertial, Martian equatorial frame.

The foregoing calculations pertain to relative grain number densities, which result from the integration of the equations of motion. In order to calculate now the absolute densities, assessments of the dust ejection rates, the dust loss mechanism, and the balance between dust income and removal are needed as discussed in the relevant papers (e.g. Krivov & Hamilton 1997). It is necessary to point out here that these assessments are subject to large uncertainties. They arise from, e.g., the inadequate knowledge of the mechanism of knocking-out the ejecta from the surfaces of Phobos and Deimos, which depends on the properties of the regolith of the moons (Murchie & Erard 1996). For these reasons the calculated absolute number densities can be in large error (Krivov & Hamilton 1997).

In the present study we use the absolute number densities of the latter authors, who give the number density $3 \cdot 10^{-12} \text{cm}^{-3}$ for the particles with radii $30 - 55 \mu\text{m}$ originating from Phobos, and the number density $5 \cdot 10^{-11} \text{cm}^{-3}$ for the particles with radii $15 - 50 \mu\text{m}$ originating from Deimos. In both cases the material density is taken $\rho = 2 \text{g cm}^{-3}$ and the radiation pressure efficiency $Q_{\text{pr}} = 1.0$. Note in this connection that $Q_{\text{pr}}/(\rho r)$ is an invariant of the equations of motion, hence comparisons of the values of radii and densities appearing in various papers should be made with reference to this quantity.

3. Optical properties of the dust grains

The most straightforward way of getting out the optical characteristics of the circummartian dust grains originating from the Martian moonlets, would seem to have them calculated from the refractive indices of Phobos' and Deimos' surface layers using, say, the Mie theory. The present knowledge of the optical properties of Phobos' and Deimos' regoliths does not allow such

calculations as it is confined only to some information on the reflectance spectra of which the so far most complete are disk-resolved data gathered by multispectral sensors VSK, KRFM and ISM from Phobos 2 (Avanesov et al. 1991; Bibring et al. 1991; Ksanfomality et al. 1991). It is not possible to return refractive indices from these data. It is also pointless, as indicated below, to assess the scattering characteristics by analogy, i.e. by looking after reflectance spectra of some known materials which resemble those of Phobos' and Deimos' surface layers.

Contrary to earlier speculations of Pang et al. (1978) the spectra of Phobos do not resemble those of carbonaceous chondrites. The closest similarities are with T-type asteroids (Murchie & Erard 1996). Not entering into details, leading beyond the scope of the present paper, the conclusion should be that among known examples of meteoritic material or asteroids there seems to be no direct spectral analogues of the Phobos' regolith in the range $200 - 3100 \text{nm}$ (Ksanfomality & Moroz 1995).

The point is know, how to proceed with the limited information on the optical properties of the Phobos surface layer at hand, in order to estimate reliably the necessary scattering characteristics (scattering phase function, scattering and extinction coefficients) of the circummartian dust grains.

Data on spectral reflectance are available as a dependence of the geometric albedo A_p on the wavelength in the spectral range $300 - 3000 \text{nm}$ (Murchie & Erard 1996). There exists a relation between A_p and the single scattering albedo $\tilde{\omega}_0$ for particles large enough to allow for clear separation between diffraction scattering and reflection with refraction. The explicit condition is $(2\pi r/\lambda) |m - 1| > 10$ where λ is the length of the wave scattered on a particle with complex refractive index m , radius r , and geometric cross section G . The condition is certainly satisfied in the visible and infrared in the size range of tens of μm we are interested in. In our calculations we shall ignore in fact the very narrow diffraction lobe, as it gives contributions to forward scattering only. We exclude the latter from our considerations because of obvious difficulties with separating it experimentally from the direct (incident) solar radiation.

Let the non-diffractive component of the scattering phase function be $p(\theta)$, where θ denotes the scattering angle. In the following $p(\theta)$ will be identified with a phenomenological phase function chosen to describe the scattering process. Then, the single scattering albedo $\tilde{\omega}_0$ can be expressed by the relation (Hanner et al. 1981):

$$\tilde{\omega}_0 = \frac{1}{2} + \frac{A_p}{2\pi p(180^\circ)} \quad (1)$$

with the normalization condition

$$\int p(\theta) d \cos \theta = \frac{1}{2\pi} \quad (2)$$

adopted here.

As the single-scattering albedo is contained in the range $1/2 \leq \tilde{\omega}_0 \leq 1$, Eq.(1) with fixed A_p (or, implicitly, with fixed λ) actually imposes a constraint on the values of the non-diffractive phase function at backscattering. Conversely, with a

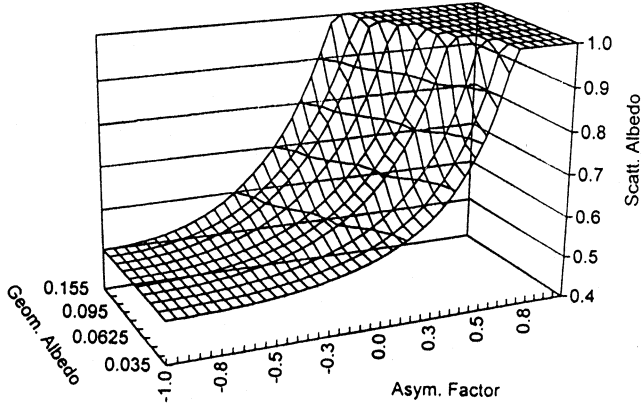


Fig. 3. Single scattering albedo $\tilde{\omega}_0$ as function of g and A_p in the case of H-G phase function. The allowed range is $1/2 \leq \tilde{\omega}_0 \leq 1$

phase function appropriately fixed, as it happens in the present study, $\tilde{\omega}_0$ for a given λ can be computed from Eq. (1). With the Henyey-Greenstein (H-G) phase function (Hulst 1980)

$$p(\theta) = \frac{1 - g^2}{4\pi (1 - 2g \cos \theta + g^2)^{3/2}} \quad (3)$$

which is among those chosen for the purpose of our assessments, Eq. (1) defines $\tilde{\omega}_0$ as a function of the asymmetry parameter g and A_p (or λ). This function is shown in Fig. 3.

The circummartian particles originating from Phobos will be then characterised by a phenomenological, non-diffractive phase function, the single-scattering albedo $\tilde{\omega}_0$ connected with the asymmetry parameter g through Eq. (1) and the extinction cross section $\sigma_{\text{ext}} = 2G$.

Among the reflectance spectra of a few small Solar System bodies acquired by the Hubble Space Telescope (Zellner & Wells 1994) these of Phobos and Deimos turn out similar, and differ from those of some asteroids. It is then plausible to assume that the optical characteristics described in the foregoing can equally apply to particles originating from Deimos.

4. Application of LOWTRAN

In the present study we concentrate on “lateral” sounding of the dust rings (edge-on, i.e. perpendicular to their symmetry axis) which could be the most suitable in the search after the thin Phobos ring. The approximation of the ring by plane-parallel layers which is a standard in the studies of, e.g., the Saturnian rings (Dones et al. 1993) clearly becomes inapplicable in this case because it leads to singularities in the expressions for scattered radiances. In order, then, to convert densities along the line-of-sight into radiances we have resorted here to the possibilities offered by the computer code LOWTRAN (Kneizys et al. 1983), originally designed to calculate atmospheric radiance for a given atmospheric path including Earth’s curvature. Consequently, LOWTRAN incorporates the effects of spatial curvature in the distributions of the medium’s characteristics. This is just the feature much desired in the calculations reported here, when the line of sounding goes across the circummartian

dust area that shows up approximate axial symmetry. The fact of using in this study a code originally designed for terrestrial atmospheric calculations may seem unusual at first sight, yet LOWTRAN has proved itself surprisingly flexible to cope with our requirements.

The diffused monochromatic radiance $I_d^\lambda(R, \mathbf{n})$ accumulated at a point R in the direction given by the unit vector \mathbf{n} in a specific medium through single scattering of the solar radiation along the line-of-sight $L(RS)$ (which is the path from the observer at R to the most distant point of scattering S taken into account) takes the form:

$$I_d^\lambda(R, \mathbf{n}) = f^\lambda \int_{L(RS)} C_s(S') p(S', \mathbf{n}_0' \cdot \mathbf{n}') \times \exp \left(\int_{L_0(S')} C_e(Q') dQ' + \int_{L(RS')} C_e(Q') dQ' \right) dS' \quad (4)$$

where f^λ denotes the monochromatic solar irradiance at the boundary of the medium, \mathbf{n}_0' is a unit vector locally pointing toward the Sun, while $L_0(S)$ denotes the path of a solar ray from the medium’s boundary to point S . The medium at point Q is optically characterised by the volume coefficients of extinction $C_e(Q)$ and scattering $C_s(Q)$, and the scattering phase function $p(Q, \mathbf{n}_0 \cdot \mathbf{n})$ where $\mathbf{n}_0 \cdot \mathbf{n} = \cos(180^\circ - \theta)$. Under normal terrestrial conditions $L_0(S)$ and $L(RS)$ are generally curved, owing to atmospheric bending of light rays. Consequently, the direction of \mathbf{n}_0' , like that of \mathbf{n}' in $p(S', \mathbf{n}_0' \cdot \mathbf{n}')$, may in general depend on the scattering point S' . LOWTRAN involves an algorithm to account for this bending. In the case of straight-line propagation (through very thin media) with assumed plane-parallel structure of the medium, Eq. (4) acquires the form well known from earlier publications (Stamnes 1986). By introducing the transmittances T_0, T, T_s corresponding to global extinction along the paths $L_0(S)$, and $L(RS)$ and to scattering along the path $L(RS)$, respectively, Eq. (4) acquires the form:

$$I_d^\lambda(R, \mathbf{n}) = f^\lambda \int_{L(RS)} \frac{T_0 T p(S', \mathbf{n}_0' \cdot \mathbf{n}')}{T_s} dT_s \quad (5)$$

To account for a possible heterogeneity of the medium, LOWTRAN allows dividing it into spherical concentric layers with slowly changing density of scatterers in each layer. The integral in Eq. (5) is then replaced by a layer-by-layer sum along the line-of-sight. For an optical path crossing N layers in a given direction, this process gives

$$I_d^\lambda(R, \mathbf{n}) = f^\lambda \sum_{j=1}^N \left\langle \frac{T_0 T p(S', \mathbf{n}_0' \cdot \mathbf{n}')}{T_s} \right\rangle_j \Delta T_{s_j} \quad (6)$$

where the quantity ΔT_{s_j} is the change of the scattering transmittance in passing through layer j , while $\langle \rangle_j$ denotes an average value for that layer. Algorithms performing the described evaluations are built into LOWTRAN.

It results from the foregoing that to the purpose of the present study, the circummartian grains are optically characterised by the extinction efficiency $Q_s = 2$ and the scattering

efficiency $Q_s = 2\tilde{\omega}_0$ with $\tilde{\omega}_0$ given by (1). As regards the non-diffractive scattering phase function $p(\cos\theta)$, for lack of quantitative knowledge about the true scattering characteristics of the grains we exploit here a range of plausible possibilities taking into account the following phase functions:

1. Henyey-Greenstein (H-G) phase function which is the prototype of anisotropic phase functions used in astrophysics (Hulst 1980), and is given by Eq (3). Within the range of values of the parameter of asymmetry g allowed by Eq. (1), the cases $g = -0.6$ and $g = -0.2$ represent moderate and weak backward scattering, whereas $g = 0.2$, representing weak forward scattering, is the largest allowed value with $\tilde{\omega}_0 \leq 1$. Note, that in virtue of Eq. (1) the increase of g from -1 to the largest possible value for a given λ makes $\tilde{\omega}_0(\lambda)$ growing from $1/2$ to 1 , which means “brightening” of the grains from “black” ($\tilde{\omega}_0 = 1/2$) to “white” ($\tilde{\omega}_0 = 1$).
2. Phase function of the zodiacal light derived from observations of the solar radiation scattered by interplanetary dust particles (IDP) at 502 nm (Lamy & Perrin 1986). The radii of the IDPs are generally believed to be contained in the range $10 - 100\ \mu\text{m}$, just as those of our circummartian grains. It is then tempting to exploit this phase function in the present study, even if the composition and size distribution of the IDPs could be different from those of the circummartian grains.

All the foregoing phase functions are here assumed independent of the scattering point, of r and of the wavelength λ of the scattered solar radiation. The assumption is supported by the comparison of Mie phase functions calculated for various materials in the spectral and size ranges discussed here (Orofino et al. 1998).

The size range of the grains and their distributions in space assumed in the present calculations, correspond to “population I” of Krivov and Hamilton (1997). The size range is then confined to $30\ \mu\text{m} < r < 90\ \mu\text{m}$ for Phobos grains and $14\ \mu\text{m} < r < 90\ \mu\text{m}$ for those of Deimos. Numerical data pertaining to the spatial distributions have been kindly provided to us by Dr. A. V. Krivov (unpublished calculations, 1996).

5. Discussion of the results

The results discussed below pertain to calculations of I_d^λ , the solar radiance scattered by the circummartian dust belts, originating from Phobos, in the following observational setups:

The observer, i.e. a sounding device aboard a spacecraft, sits on the X axis at a point with the coordinate $x = +5$ Martian radii (see Fig. 4). “Sounding” is carried on over the whole relevant range of angle φ subtended at the observer by the segment of the X axis directed towards Mars, and by the line-of-sight. At a given epoch, i.e. with a fixed position of the Sun, scanning over φ leads to variations of the scattering angle θ . Alternatively, with fixed φ (fixed line-of-sight) the scattering angle θ varies over the Martian year, as the dust area revolves about the Sun.

The line-of-sight lies in the equatorial plane of Mars, which is the most appropriate to detect the radiance scattered by the

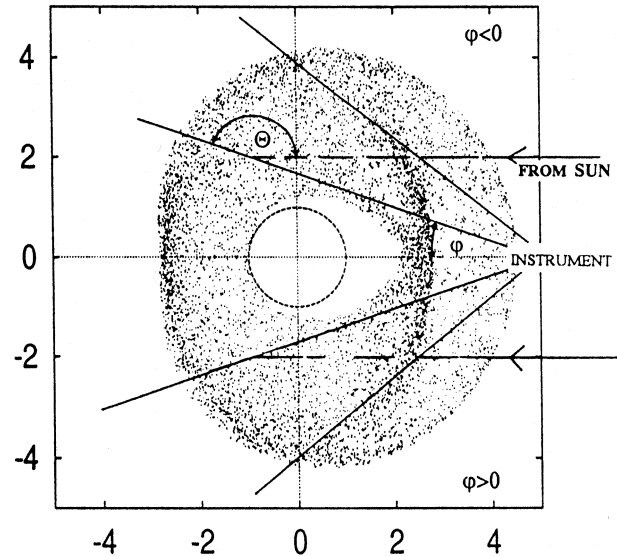


Fig. 4. The observational setup overlaying the XY projection of the Phobos’ torus (see Fig. 1) showing the azimuthal angles φ and the scattering angles θ of a few lines-of-sight

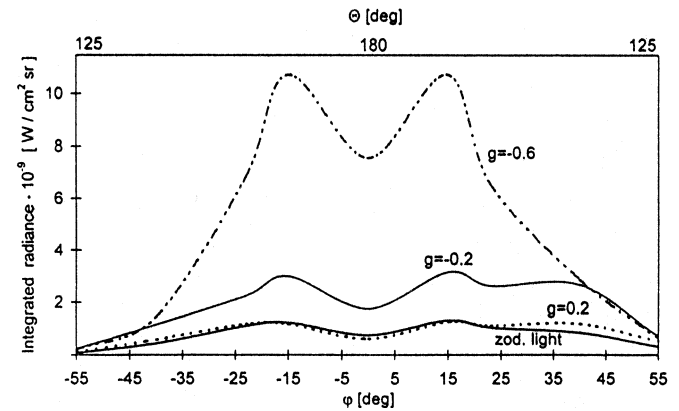


Fig. 5. The integrated radiance I_d scattered by the $32\ \mu\text{m}$ particles of the Phobos’ torus at the vernal equinox versus the scattering angle θ and the azimuthal angle φ

Phobos ring (see Fig. 1). The way of carrying on the “sounding” implies that the angular field of view of the sounding device is very narrow so that no scattered radiation enters the device from outside the close neighbourhood of the equatorial plane. To the purpose of calculating the volume coefficients of extinction C_e and scattering C_s (both depending on the spatial density of the grains) the line-of-sight is divided into 6 segments corresponding to the division of the dust area into layers, as required by LOWTRAN. The values of the density at the boundaries of the segments along the line-of-sight are input data depending on the angle φ and the epoch. The calculated scattered radiance I_d^λ is then integrated over the wavelength interval $0.35 - 1.0\ \mu\text{m}$ which spans about $2/3$ of the “solar constant”. The range of integration could be intended as a typical spectral range of a sounding device (photometer) operating in the VIS and adjacent spectral regions. The integrated I_d as function of angle φ and of the scattering angle θ at 4 epochs (vernal and autumn-

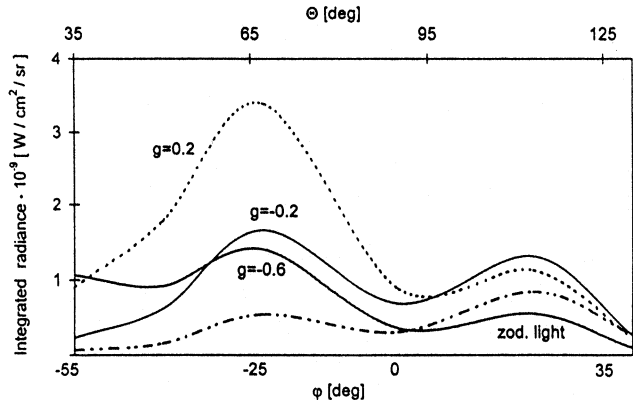


Fig. 6. Same as Fig. 5 but at the summer solstice

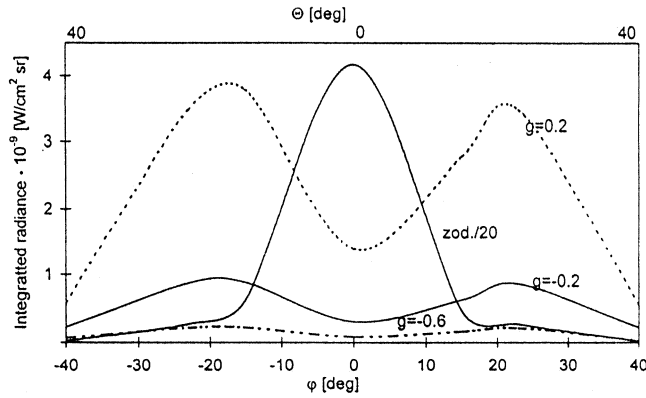


Fig. 7. Same as Fig. 5 but at the autumnal equinox

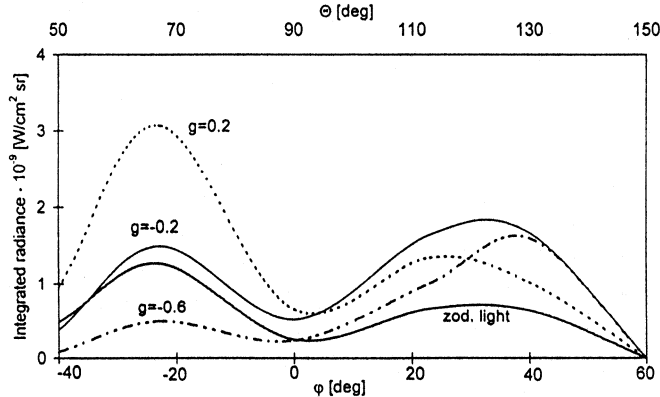


Fig. 8. Same as Fig. 5 but at the winter solstice

nal equinoxes, summer and winter solstices) for grains with $30 \mu\text{m} < r < 35 \mu\text{m}$ (of highest number density along the line-of-sight) and for various phase functions is shown in Figs. 5–8. They correspond to the first observational setup, as described before.

Vernal and autumnal distributions of I_d span the ranges of the scattering angle $\theta > 125^\circ$ centered at $\theta = 180^\circ$ in the backward hemisphere and $\theta < 40^\circ$ centered at $\theta = 0^\circ$ in the forward hemisphere, respectively. The corresponding ranges of the summer and winter distributions span the range $\sim 30^\circ < \theta < 150^\circ$ centered at $\theta = 90^\circ$. Three main factors contribute, to various

extent, to the angular dependence of I_d for different phase functions. These are: the variation of the optical thickness along the line-of-sight with φ , the variation of the phase function with θ and the dependence of Q_s on the choice of the phase function in accordance with Eq. (1). The values of the optical thickness along the line-of-sight at a given epoch display a saddle-shaped variation with angle φ , centered at $\varphi = 0^\circ$, showing up steep peaks around $\varphi = \pm 20^\circ$ and steep falls beyond. In the vernal and autumnal epochs the heights of the twin peaks are almost equal. In summer and winter the peak at $\varphi = 20^\circ$ is lower from its counterpart by a factor of about 3/4. This functional shape visibly affects the angular variation of I_d shown in Figs. 5–8 because the optical thicknesses around the peaks vary with φ at a much higher rate than the phase functions in the corresponding ranges of θ . An important exception is radiation scattered around $\theta = 0^\circ$, exemplified by the autumnal distribution (see Fig. 7) where the sharp forward peak of the phase function of the zodiacal light overwhelms the variation of the optical thickness.

In view of the foregoing, the approximate symmetry of the vernal and autumnal distributions of I_d about $\varphi = 0^\circ$ comes as no surprise (Figs. 5 and 7). The exceptionally high forward signal ($I_d = 8.34 \cdot 10^{-8} \text{ W cm}^{-2} \text{ sr}^{-1}$) is associated with the phase function of the zodiacal light ($Q_s \approx 1.35$). The comparison of the vernal and autumnal I_d associated with H-G phase functions shows that the dependence of its magnitude upon the asymmetry parameter g is stronger than upon Q_s , the correlated scattering efficiency of the grains. The largest signal in the vernal case ($I_d = 1.07 \cdot 10^{-8} \text{ W cm}^{-2} \text{ sr}^{-1}$) is associated with $g = -0.6$ describing moderate backward scattering, despite low scattering efficiency ($Q_s \approx 1.0$). The largest autumnal signal ($I_d = 3.78 \cdot 10^{-9} \text{ W cm}^{-2} \text{ sr}^{-1}$) is associated with $g = 0.2$ describing weak forward scattering, and results from about the same number of scatterers along the line-of-sight as in the foregoing vernal case. Yet, it is almost 3 times smaller, despite larger scattering efficiency ($Q_s \approx 1.4$). Also this autumnal signal is only slightly larger than the vernal signal associated with $g = -0.2$ what reflects the equality of the phase functions and the relation between the values of Q_s in both cases.

A different picture emerges from summer and winter distributions of I_d (Figs. 6 and 8). Its largest values attain $I_d = 3.39 \cdot 10^{-9} \text{ W cm}^{-2} \text{ sr}^{-1}$ in summer and $I_d = 3.07 \cdot 10^{-9} \text{ W cm}^{-2} \text{ sr}^{-1}$ in winter, both associated with the H-G phase function with $g = 0.2$. Here, the gable of the distribution of the optical thickness at $\varphi > 0$ is suppressed with respect to the gable at $\varphi < 0$ what leads to a reduction of I_d in the $\varphi > 0$ range as compared to its $\varphi < 0$ counterpart. It is evident that in the relevant interval of θ the overall decrease of the phase functions with $g > 0$ brings an additional damping of I_d . As to the phase functions with $g < 0$ their overall growth with θ only hardly compensates the reduction of I_d caused by a suppression of the optical thicknesses at $\varphi > 0$.

The behaviour of the magnitude of I_d at $\varphi = 0^\circ$ during the Martian year is shown in Fig. 9. This is an example of the second observational setup discussed before, when the position of the sounding device is fixed in the Martian inertial frame, and the scattering angle changes on account of the motion of

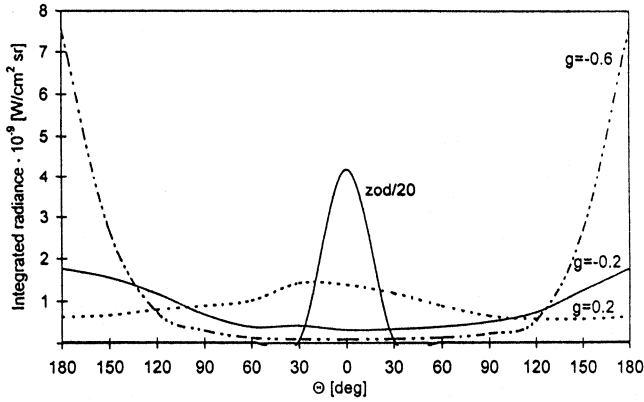


Fig. 9. The integrated radiance I_d scattered by the $32 \mu\text{m}$ particles of the Phobos' torus at $\varphi = 0^\circ$ versus θ during the Martian year

the dust belts about the Sun. The variations of I_d with θ are driven mainly by the angular dependence of the phase functions and are only weakly modified by small seasonal changes of the optical thickness along the line-of-sight.

In order to evaluate now the total radiance scattered by the Phobos dust grains in the relevant size range $30 \mu\text{m} < r < 90 \mu\text{m}$ we assessed the number densities along a line-of-sight in the relevant size subranges $10 - 15 \mu\text{m}$ wide (A. V. Krivov, unpublished calculations 1996) and their contributions to the total number density. The evaluation leads to the conclusion that the ratio of the total scattered radiance to that scattered by the grains in the $30 - 35 \mu\text{m}$ size range can be very satisfactorily approximated by 1.5. The same evaluation carried on for the Deimos grains tells that the total radiance scattered in the size range $17 \mu\text{m} < r < 90 \mu\text{m}$ is, to a good approximation, 10 times larger than the total radiance scattered by the Phobos grains. All evaluations pertain, of course, to radiances scattered in the Martian equatorial plane and its immediate neighbourhood.

6. Conclusions

The largest values of the calculated total radiance scattered by the Phobos and Deimos belts along the Martian equatorial plane are displayed in Table 1. This setup gives, first, an estimate of the signal that can be expected during photometric searches after the Martian dust belts and, second, indicates the best seasons for looking after the dust with a specific choice of a scattering phase function.

We note then, that the expected signal can, in general, attain the order of $10^{-8} \text{ W cm}^{-2} \text{ sr}^{-1}$, a value by no means critical for a today's good, sensible photometer. In fact, the "torometer" in the payload of the ill-fated Mars'96 mission (Hirsch et al. 1996) was expected to pick out signals as low as $2 \cdot 10^{-9} \text{ W cm}^{-2} \text{ sr}^{-1}$.

There are two even more favourable observational setups, yielding signals considerably above the foregoing average level. These are the spring season in case of backscattering particles producing a signal of the order of $10^{-7} \text{ W cm}^{-2} \text{ sr}^{-1}$, and the autumn season in case of strongly forward scattering grains sim-

Table 1. Maximum values of the integrated radiance jointly scattered by the Phobos' and Deimos' tori over all seasons and all considered phase functions

phase function	spring	summer	autumn	winter
H-G, $g = -0.6$	$1.8 \cdot 10^{-7}$	$1.4 \cdot 10^{-8}$	$3.6 \cdot 10^{-9}$	$2.6 \cdot 10^{-8}$
H-G, $g = -0.2$	$5.2 \cdot 10^{-8}$	$2.8 \cdot 10^{-8}$	$1.5 \cdot 10^{-8}$	$2.8 \cdot 10^{-8}$
H-G, $g = +0.2$	$2.1 \cdot 10^{-8}$	$5.6 \cdot 10^{-8}$	$6.3 \cdot 10^{-8}$	$5.1 \cdot 10^{-8}$
zodiacal light	$2.2 \cdot 10^{-8}$	$2.3 \cdot 10^{-8}$	$1.4 \cdot 10^{-6}$	$2.1 \cdot 10^{-8}$

ilar to interplanetary dust particles of the zodiacal light, when the signal could attain $10^{-6} \text{ W cm}^{-2} \text{ sr}^{-1}$.

The foregoing assessments indicate therefore, that photometric searches after the Martian dust belts augur well, and should be undertaken during the forthcoming Martian missions.

Acknowledgements. Our thanks go to Alexander Krivov of St. Petersburg University, Russia, for providing us with his unpublished numerical data relative to space distributions of grains in the Martian dust rings, and for introducing us patiently into the details of his calculations. The contribution of Vincenzo Orofino of the University of Lecce, Italy, to the computation of the normalized phase function of the zodiacal light particles is appreciated. This research was supported by the Polish State Committee for Scientific Research under grant No 2P03C01010.

References

- Avanesov G., Zhukov B., Ziman V., et al., 1991, *Planet. Space Sci.* 39, 281
- Bibring J.-P., Langevin I., Moroz V. I., et al., 1991, *Lunar Planet. Sci.* XXII, 99
- Dones L., Cuzzi J. N., Showalter M. R., 1993, *Icarus* 105, 184
- Hamilton D. P., 1996, *Icarus* 119, 153
- Hanner M. S., Giese R. H., Weiss K., Zerull R., 1981, *A&A* 104, 42
- Hirsch H., Formisano V., Moroz V. I., et al., 1996, *Planet. Space Sci.* 44, 889
- Hulst H. C. van de, 1980, *Multiple Light Scattering*, Academic Press, New York
- Kneizys F. X., Shettle E. P., Abreu L. W., et al., 1988, *Users Guide to LOWTRAN7*, Air Force Geophys. Lab., Hanscom AFB, MA, USA, Rep. AFGL-TR-83-0187
- Krivov A. V., 1994, *A&A* 291, 657
- Krivov A. V., Hamilton D. P., 1997, *Icarus* 128, 335
- Krivov A. V., Sokolov L. L., Dikarev V. V., 1996, *Celest. Mech. Dynam. Astron.* 63, 313
- Ksanfomality L., Moroz V. I., 1995, *Icarus* 117, 383
- Ksanfomality L., Murchie S., Britt D., et al., 1991, *Planet. Space Sci.* 39, 311
- Lamy P. L., Perrin J.-M., 1986, *A&A* 163, 269
- Murchie S., Erard S., 1996, *Icarus* 123, 63
- Orofino V., Grygorczuk J., Jurewicz A., 1998, *Planet. Space Sci.* in press
- Pang K., Pollack J. B., Veverka J., et al., 1978, *Sci.* 199, 64
- Stamnes K., 1986, *Rev. Geophys.* 24, 299
- Zellner B., Wells E. N., 1994, *Lunar Planet. Sci.* XXV, 1541